



HAL
open science

How Symmetry Influences the Dissociation of Protonated Cyclic Peptides

Ariel F Pérez-Mellor, Riccardo Spezia, Anne Zehnacker

► **To cite this version:**

Ariel F Pérez-Mellor, Riccardo Spezia, Anne Zehnacker. How Symmetry Influences the Dissociation of Protonated Cyclic Peptides. *Symmetry*, 2022, 14 (4), pp.679. 10.3390/sym14040679 . hal-03736143

HAL Id: hal-03736143

<https://hal.science/hal-03736143>



Submitted on 22 Jul 2022

HAL is a multi-disciplinary open access archive for the deposit and dissemination of scientific research documents, whether they are published or not. The documents may come from teaching and research institutions in France or abroad, or from public or private research centers.

L'archive ouverte pluridisciplinaire **HAL**, est destinée au dépôt et à la diffusion de documents scientifiques de niveau recherche, publiés ou non, émanant des établissements d'enseignement et de recherche français ou étrangers, des laboratoires publics ou privés.

Review

How Symmetry Influences the Dissociation of Protonated Cyclic Peptides

Ariel F. Pérez-Mellor ^{1,2,†} , Riccardo Spezia ^{2,*}  and Anne Zehnacker ^{1,*}

¹ CNRS, Institut des Sciences Moléculaires d'Orsay, Université Paris-Saclay, 91405 Orsay, France; ariel.perez-mellor@unige.ch

² Laboratoire de Chimie Théorique, Sorbonne Université, UMR 7616 CNRS, 4, Place Jussieu, 75005 Paris, France

* Correspondence: riccardo.spezia@sorbonne-universite.fr (R.S.);

anne.zehnacker-rentien@universite-paris-saclay.fr (A.Z.)

† Current affiliation: Department of Physical Chemistry, University of Geneva, 1211 Geneva, Switzerland.

Abstract: Protonated cyclic dipeptides undergo collision-induced dissociation, and this reaction mechanism strongly depends on the symmetry and the nature of the residues. We review the main dissociation mechanism for a series of cyclic dipeptides, obtained through chemical dynamics simulations. The systems range from the symmetrical cyclo-(glycyl-glycyl), with two possible symmetrical protonation sites located on the peptide ring, to cyclo-(tyrosyl-prolyl), where the symmetry of protonation sites on the peptide ring is broken by the dissimilar nature of the different residues. Finally, cyclo-(phenylalanyl-histidyl) shows a completely asymmetric situation, with the proton located on one of the dipeptide side chains, which explains the peculiar fragmentation mechanism induced by shuttling the proton, whose efficiency is strongly dependent on the relative chirality of the residues.

Keywords: chirality; mass spectrometry; chemical dynamics; quantum chemistry



Citation: Pérez-Mellor, A.F.; Spezia, R.; Zehnacker, A. How Symmetry Influences the Dissociation of Protonated Cyclic Peptides. *Symmetry* **2022**, *14*, 679. <https://doi.org/10.3390/sym14040679>

Academic Editors: Mateo Alajarin and Stefano Superchi

Received: 20 February 2022

Accepted: 22 March 2022

Published: 25 March 2022

Publisher's Note: MDPI stays neutral with regard to jurisdictional claims in published maps and institutional affiliations.



Copyright: © 2022 by the authors. Licensee MDPI, Basel, Switzerland. This article is an open access article distributed under the terms and conditions of the Creative Commons Attribution (CC BY) license (<https://creativecommons.org/licenses/by/4.0/>).

1. Introduction

Symmetry plays an important role in nature, from the macroscopic world to cosmology and high-energy physics. In particular, it is possible to classify molecules according to their symmetry or lack thereof. Beyond this, symmetry plays an essential role in molecular structure and reactivity. To a large extent, it dictates the rules that govern spectroscopy, i.e., the absorption and emission of light, or photophysics, i.e., the fate of molecules after light absorption [1]. For example, homonuclear diatomic molecules, such as N₂ or O₂, are prohibited from absorbing IR radiation, which is fortunate, since they are the main constituents of the atmosphere. UV absorption by the highly symmetric benzene molecule is much weaker than absorption by its less symmetrical substituted derivative. Symmetry also influences chemical reactivity. For example, the well-known Woodward–Hoffmann rules that govern concerted thermal and photochemical reactions involving a cyclic transition state are based on the symmetry of the frontier orbitals of the reagents [2]. A peculiar aspect of symmetry, or rather dissymmetry, is chirality, which is the property of a molecule to not be superimposable on its mirror image. The foundations of chirality were laid at the beginning of the 19th century, when a French physicist, J.B. Biot, discovered that certain organic substances in solution rotate the plane of polarization of linearly polarized light. However, the decisive step was provided by L. Pasteur; he proposed that this property was molecular in nature, and was intimately related to life. The concept was completed when Lord Kelvin named this property “chirality”. Le Bel and van't Hoff proposed the asymmetric carbon, substituted by four different types of atoms or groups, as a source of chirality [3]. In general, chiral molecules belong to one of the following point groups: C₁, C_n or D_n.

Chirality is pervasive in biomolecules. All natural amino acids, the constituents of proteins, with the exception of glycine, possess an asymmetric carbon atom, also called a stereogenic center, which always has an L absolute configuration (Figure 1).

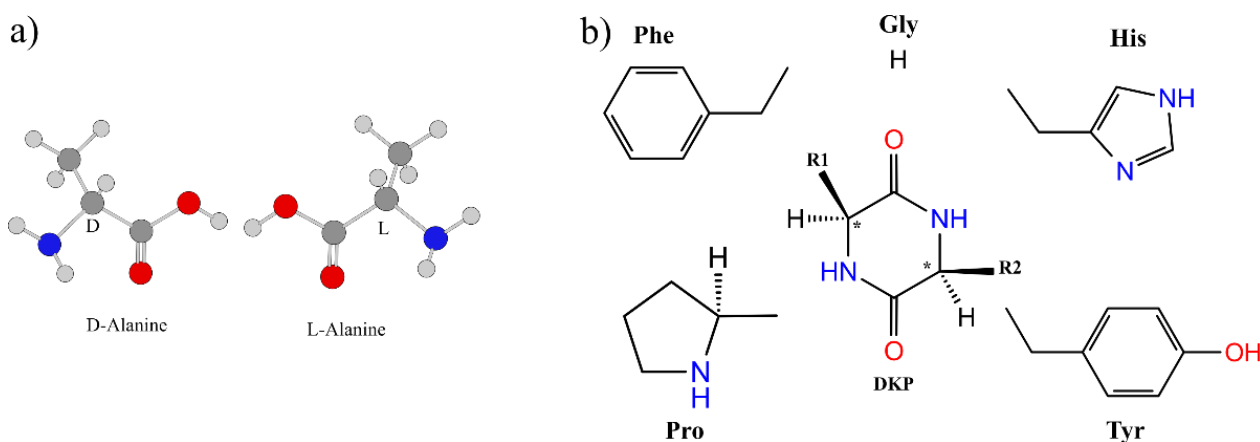


Figure 1. (a) The two enantiomers of alanine. (b) DKP dipeptides, involving glycine (Gly), phenylalanine (Phe), tyrosine (Tyr), histidine (His), or proline (Pro), depending on R1 and R2. *c*-Gly-Gly is obtained for R1 and R2 = H. Stereogenic centers are marked with *.

Peptides arise from the fusion of amino acids, resulting in the creation of a peptide bond and the loss of water, with no modification of the stereogenic center. For this reason, the natural peptides also have an L configuration. Intramolecular peptide bond formation results in cyclic peptides, also called diketopiperazine (DKP) peptides, from the name of the cycle. They are important as by-products of sweetener degradation or for their potential applications as drugs [4]. In contrast to biosynthesis, chemical engineering allows the synthesis of cyclic dipeptides with different absolute configurations of the stereogenic carbon atoms. In the past few years, we have undertaken a spectroscopic study of cyclic dipeptides with identical or opposite configurations of the residues, to assess the influence of chirality on their structure and reactivity [5–13]. We have resorted to IR spectroscopy under jet-cooled or ion trap conditions, aided by quantum chemical calculations, to determine the structure of the neutral or protonated molecules. In addition, we have rationalized the collision-induced dissociation mechanism of the protonated peptides in an ion trap, by means of chemical dynamics calculations. Here, we will focus on the latter aspect, and we will describe how symmetry influences this mechanism. To this aim, three systems are considered that differ in the substituent of the C_{α} atoms (C_1^{α} and C_3^{α}) (Figure 1), and by their symmetry. In what follows, the peptides will be denoted by *c*-AB, where *c* stands for cyclic and A or B is the usual notation for the amino acid residue. We will start with the most simple and symmetrical *c*-Gly-Gly molecule. In the crystal, it is centrosymmetric and belongs to the C_{2h} symmetry group because the DKP ring is planar, and all substituents of C_1^{α} and C_3^{α} are hydrogen atoms (Figure 2) [14].

In contrast to the solid-state structure, there is no symmetry plane in the gas-phase structure, which has C_2 symmetry [15]. Therefore, *c*-Gly-Gly exists as a pair of two fast-interconverting enantiomers, which manifests itself as splitting of the rotational transitions [16]. The planar transition state separating the two fast-interconverting enantiomers has an inversion center (*i*) and is not chiral; it can be viewed as a “time-averaged” structure. The addition of a proton results in the loss of the inversion center and the C_2 symmetry axis [17]. Moreover, there are two equivalent sites for the proton to bind—the two CO groups. As a result, the macroscopic system can be viewed as the contribution of molecules protonated on either of these sites. The substitution of the C_{α} atoms lowers the symmetry, even if the two substituents are identical, such as in *c*-Phe-Phe, as shown in Figure 3. The main reason is that chirality is brought about by the substitution of C_1^{α} and C_3^{α} . Different cases are encountered, depending on the relative absolute configuration of the residues and their nature. When one residue is L and the other D, the symmetry group may be

C_i (with the inversion center as the only symmetry element) or C_1 (no symmetry at all). Achiral C_i conformers are observed for example in *c*-DAla-LAla, in which one methyl group pointing upwards, relative to the peptide plane, and the other pointing downwards [18]. When both conformers are *L*, the symmetry group may be C_2 (two-fold symmetry axis as the only symmetry element) or C_1 . The C_1 structures in which the two substituents have non-equivalent orientations are commonly observed in either LL or LD structures containing an aromatic ring, as shown in Figure 3. The most common geometry consists of one substituent folded on the DKP ring and the other extended outside. This happens for *c*-Phe-Phe in its most stable neutral or protonated forms. The so-called stacked geometry, where two aromatic rings face each other, belongs to the C_2 symmetry point group; this is an observed stable form of *c*-LTyr-LTyr in the gas phase. A similar sandwich-like structure was also proposed for *c*-LTyr-LPhe in polar solution [19]. Its diastereomer *c*-LTyr-DPhe has two rings folded over the DKP ring in polar solution, on each side of the peptide ring [20]. All these C_1 or C_2 conformations are chiral. In conditions where conformational flexibility is possible (high temperature), this type of chirality is transient, because the substituents can easily go from folded to extended orientations, and vice versa. However, it is permanently chiral at low temperatures because the molecular motions are frozen. When protonation happens on the CO group, such as in the abovementioned systems, it has little effect on the symmetry [8]. For dipeptides built from two identical residues, protonation breaks the C_i symmetry of the LD systems, but the two CO are equivalent. For the LL systems, the C_2 conformations remain C_2 and the two CO are equivalent (see Figure 2a). In contrast, for the C_1 conformations (no symmetry element), the two protonation sites are not equivalent; either the CO of the folded residue or that of the extended residue is protonated. However, as mentioned before, rapid interconversion happens between the extended and folded positions at room temperature. Finally, *c*-Phe-His shows completely different properties. As the two residues are different, the system has no symmetry (C_1), no matter the conformation. Moreover, protonation happens on the imidazole ring of His, which further dissymmetrizes the molecules, in terms of charge distribution.

In this article, we explore how symmetry affects the collision-induced dissociation (CID) of protonated cyclic dipeptides. We propose an analysis based on the symmetry of the proton migration pathway that rationalizes the fragmentation of cyclic dipeptides, depending on their symmetry properties. We start from the most symmetrical *c*-Gly-Gly molecule, which is taken as a paradigm. We then extend the discussion to *c*-Phe-Phe and *c*-Phe-His. To this end, we model the collision-induced dissociation efficiency along different reactive paths and compare them to experimental values. Finally, we show how symmetry, or lack thereof, along these reaction paths affects the difference in fragmentation between LL and LD.

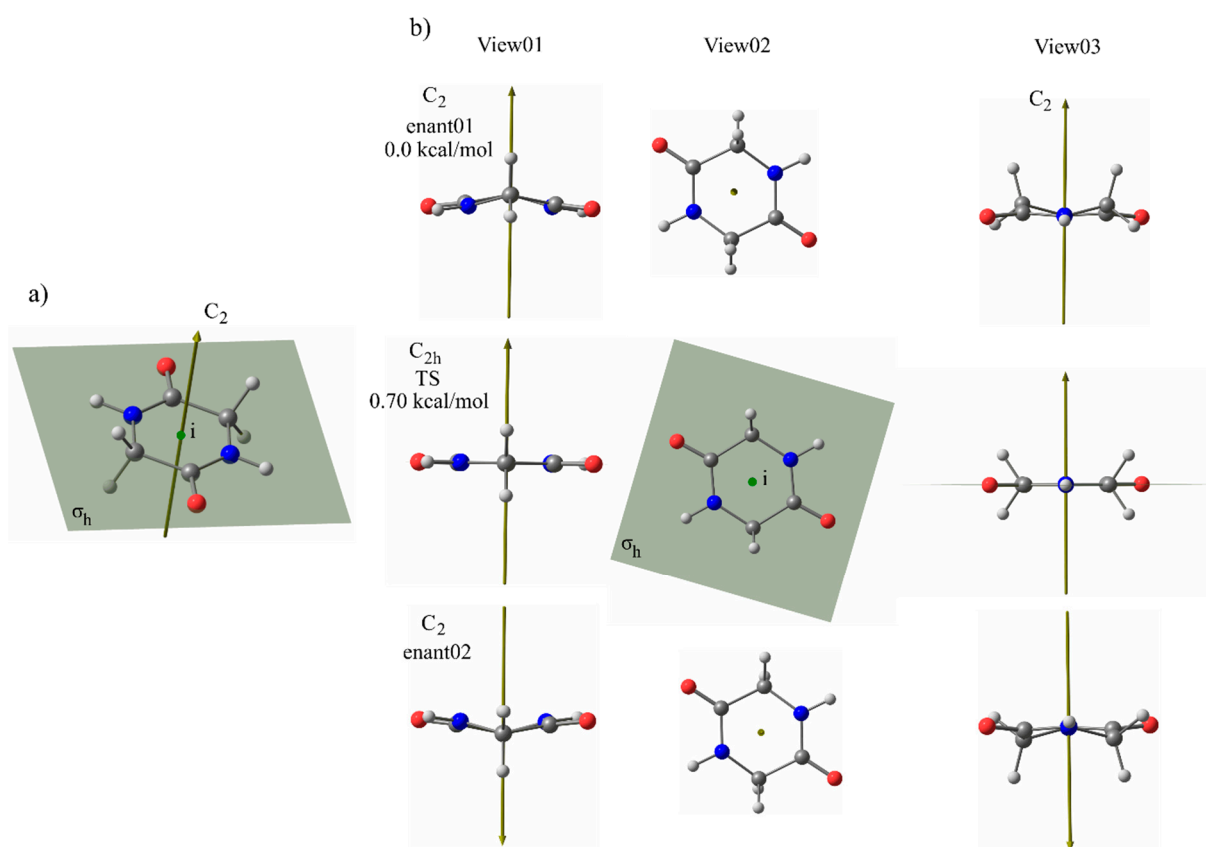


Figure 2. (a) Symmetry elements of the DKP ring, with i denoting the inversion center, σ_h the symmetry plane, and C_2 the symmetry axis for a rotation of π . (b) Different views of the most stable enantiomeric conformers of *c*-Gly-Gly and the planar (symmetrical) transition state separating them. The relative energies are calculated at the DFT level (see text).

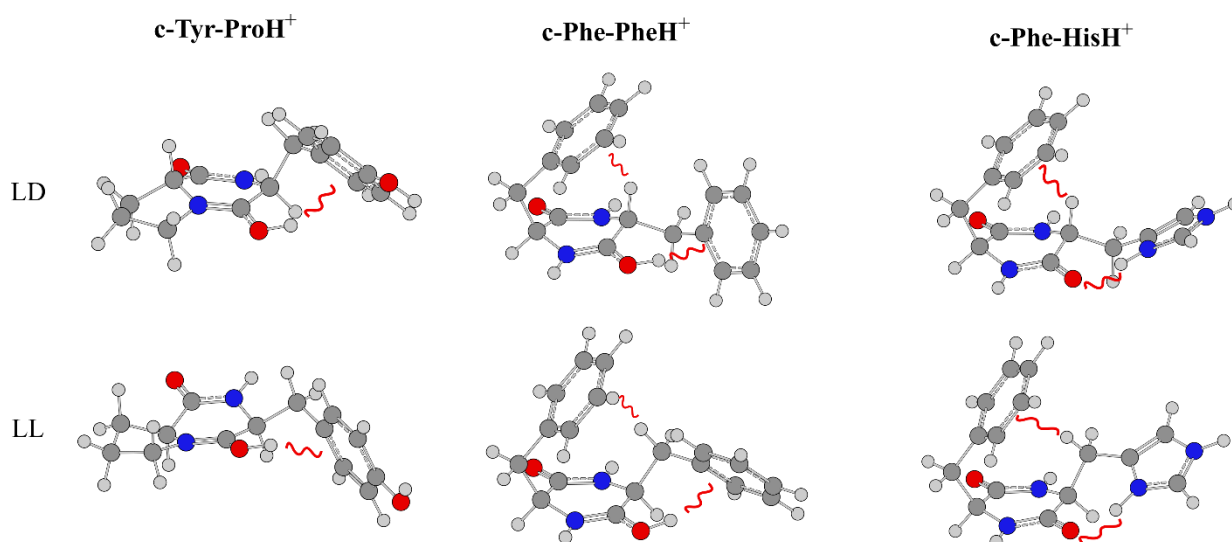


Figure 3. Most stable structures of the DKP dipeptides discussed in this review. The $\text{OH}^+ \dots \pi$, $\text{CH} \dots \pi$, $\text{NH}^+ \dots \text{O}$, hydrogen bond interactions are indicated by the curly red line (see text).

2. Experimental and Theoretical Methods

2.1. Experimental Methods: Collision-Induced Dissociation

This work rests on multistage mass spectrometry experiments using a Fourier transform ion cyclotron resonance (7T FT-ICR hybrid mass spectrometer Bruker, Apex Qe)

mass spectrometer [21]. They have been performed at the SMAS (Spectrométrie de Masse, Analyse et Spectroscopie) facility at the Centre Laser Infrarouge d'Orsay (CLIO) [22]. They consist of three steps, as depicted in Figure 4.

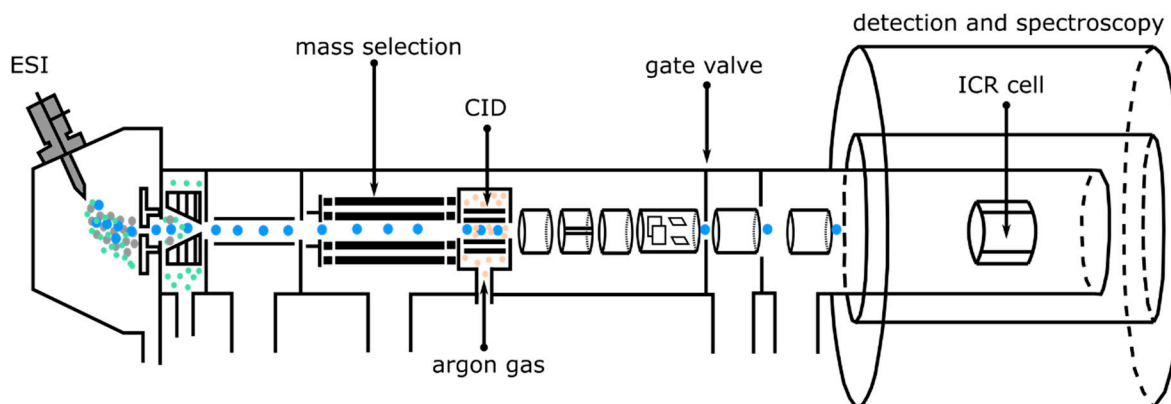


Figure 4. Principle of the mass spectrometry experiment, with (from left to right) the production, mass selection collision-induced dissociation, and analysis steps. See text for the description of the different elements.

The first step delivers the protonated molecules from a dilute solution to the gas phase, thanks to the soft ionization obtained in an electrospray ion source (ESI). The second part encompasses a linear quadrupole, where the ions are sorted according to their mass-to-charge ratio m/z , and a linear hexapole ion trap, where they are accumulated for a duration of 1 s. They undergo collisions with argon, which results in collision-induced dissociation (CID). CID is a powerful tool that has been widely applied to the structural study of peptides [23,24]. The collision energy can be varied by modifying the kinetic energy of the ions. This is performed by tuning the voltage applied on the rods of the ion trap. The ions are then transferred to the ICR cell, where they are trapped by the combination of electric and magnetic fields. The latter allows the detection of the CID fragments according to their m/z .

The dipeptides were obtained from Novopep (China) (98% purity) and used as provided.

2.2. Theoretical Methods—Fragmentation Simulations

The nature of the fragments experimentally observed in CID can be obtained from simulations, independently from the experiments. This is the so-called theoretical MS/MS [25], which is based on chemical dynamics simulations and, in particular, on the pioneering studies of Hase and co-workers [26]. The results obtained can, thereby, be advantageously compared to the experimental results on peptide fragmentation [23,27–32]. Methods and applications were recently reviewed by Hase, Spezia, and co-workers [33,34]. Therefore, here, we will only give the general principles of the methodology we use to understand the fragmentation properties of chiral protonated peptides from chemical dynamics simulations [10,35].

Each structure was first optimized at the B3LYP/DFT/6-311++g(d,p)/D3 level of theory [36,37], and the vibrational spectra were calculated [38] and compared with IR spectra obtained by infra-red multiple-photon dissociation (IRMPD) experiments. The calculated conformer that best reproduced the experiment was chosen as the initial structure used in the simulations. Next, simulations were run using the RM1-D semi-empirical Hamiltonian [39,40], which is a good compromise between computational time and accuracy. Each ion was then optimized at the RM1-D level of theory and activated through microcanonical normal mode sampling [41], with given energies in the 367–617 kcal/mol range. These excess energies are enough for the ion to fragment and react sufficiently in the given simulation time. On the other hand, the energies are not too high, so as to avoid an unphysical sudden breaking. Therefore, an ensemble of trajectories was propagated for each energy value, typically between 3000 and 11,000, each 20–25 ps long, depending on the energy and

the system. Table S1 of the Supplementary Information (SI) summarizes all the simulation details for c-Tyr-ProH⁺ and c-Phe-HisH⁺. Information for c-Gly-GlyH⁺ can be found in previously published work [13].

The internally activated system evolves following the Newton equation of motions, integrated numerically using the velocity Verlet algorithm [42], with a 0.1 fs time step, ensuring energy conservation. The trajectories are monitored to observe if a reaction has occurred. It is important to notice that this direct approach does not impose any reaction product or mechanism; the products obtained in fine result from the simulations, given the initial conditions and the way energies and forces are calculated (in the present case at the RM1-D level of theory).

Trajectories are propagated in Cartesian coordinates, and for such complex systems, it is impossible to know all the possible products in advance. Therefore, we used a graph-theory-based approach to analyze them automatically [13]. This approach can also identify the ion–molecule complexes that are often transient structures in CID processes.

Microcanonical rate constants were extracted from the molecular dynamics simulations using the method described previously [13]. Briefly, the primary fragmentation of the peptides is described by the evolution of three states, namely, the starting point (S), intermediate (I), and primary fragmentation product (P) states. In this three-stage model, the intermediate state encapsulates all the possible geometries of the systems before their fragmentation [13]. This allows for the determination of the effective microcanonical rate constants, corresponding to the transformation from starting point to intermediate and vice versa, and from the starting point and intermediate to the final fragmentation state.

The last step consists of extracting the threshold energies using the classical Rice–Ramsperger–Kassel (RRK) [43] theory from the energy dependence of the effective rate constants, as follows:

$$k_{ij}(E) = \nu^{ij} \left(1 - \frac{E_a^{ij}}{E} \right)^{s-1}$$

where ν , s , and E_a are the effective frequency, the number of vibrational degrees of freedom of the reactant, and threshold energy, respectively, with i and j being S, I, or P.

All simulations were performed with the VENUS chemical dynamics software [44], which is coupled with Mopac5.022 mn [45]. Analyses were performed with our graph theory code developed in-house [13].

3. Results and Discussion

3.1. Experimental Results on the Fragmentation of Diketopiperazine Peptides

The structure of the protonated dipeptides under study was determined by comparing the vibrational spectra obtained by IRMPD with those simulated for the most stable calculated structures. In all the systems, but c-Phe-HisH⁺, the proton is located on the peptide CO. In c-Gly-GlyH⁺ or c-Ala-AlaH⁺, the two CO are equivalent [17,46], which is not the case in c-Phe-PheH⁺, despite the identical aromatic substituents. Dissymmetry is brought upon by the non-equivalent position of the two aromatic rings [5]. Indeed, one of them is extended, which allows it to interact with the CO, and the other is folded over the DKP ring (see Figure 3). Due to the different substituents, the two CO are not equivalent in c-Tyr-ProH⁺ [35]. The previously obtained results indicate that protonation on the oxygen atom of the Tyr residue is energetically favorable (see Figure 4).

Experimental data are available for the fragmentation of protonated DKPs, such as c-Gly-GlyH⁺, c-Ala-AlaH⁺, and c-Ala-GlyH⁺, and more complex DKPs, such as c-Tyr-ProH⁺, c-Phe-PheH⁺, and c-Phe-HisH⁺ [17,46–48]. The role of the stereochemistry of the residues has been studied for the last three systems. The CO loss is the dominant process in all systems. The loss of the NH₃ neutral fragment is much weaker. It is either not observed or negligible in all four systems, except c-Phe-HisH⁺, where it is significant. In what follows, we will focus on CO loss, which is common to all the DKP-based dipeptides studied so far,

with, however, very different sensitivity to chirality, depending on the system, as shown in Figure 5 on the example of *c*-Tyr-ProH⁺ and *c*-Phe-HisH⁺ [13,35].

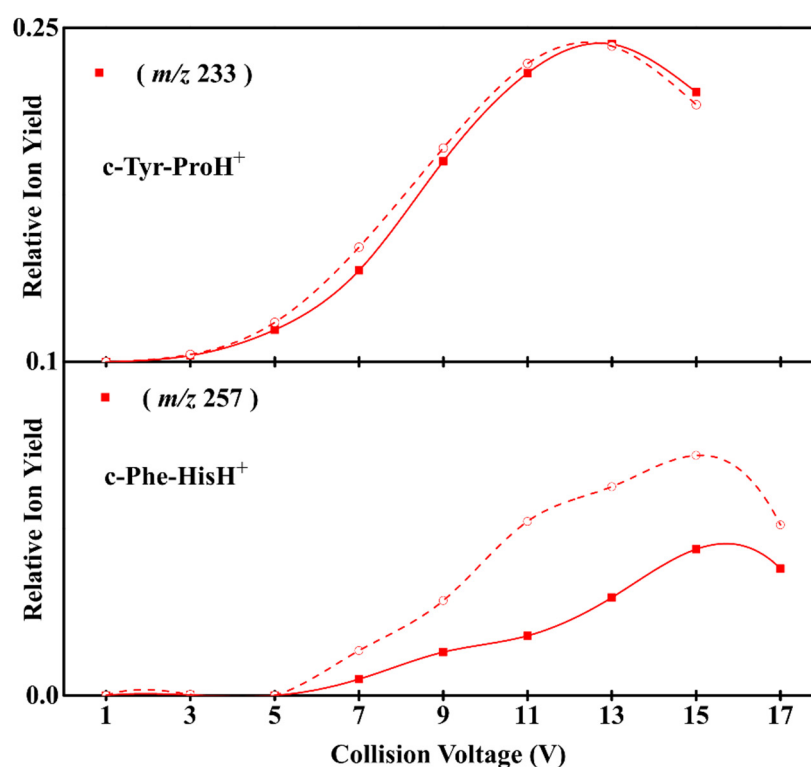


Figure 5. Experimental relative fragmentation yield for CO loss for protonated LL (continuous lines and squares) and LD (dashed lines and circles) for protonated *c*-Tyr-Pro and *c*-Phe-His.

We can distinguish two families. Firstly, *c*-Tyr-ProH⁺, where the proton is located on the amide CO, shows little or no enantioselectivity in its fragmentation patterns [35]. Both the total fragmentation and CO loss yield are very similar for the LL and LD stereoisomers. Very little effect of chirality is also observed in the CID of *c*-Phe-PheH⁺ [5]. In contrast, *c*-Phe-HisH⁺, for which the proton is located on the imidazole, shows strong enantioselectivity, which we will rationalize in what follows.

3.2. Sidechain Effect on Primary Fragmentation of Diketopiperazine Peptides

We theoretically evaluated the effect of the residue on the effective microcanonical rate constant of three diketopiperazine peptides, namely, *c*-Gly-GlyH⁺, *c*-Tyr-ProH⁺, and *c*-Phe-HisH⁺, for which only the LL diastereomer was considered. The same kinetic temperature range was used for the three systems to facilitate the comparison. In all cases, the starting point is the most stable geometry, except for *c*-Phe-HisH⁺, where we also included the structures with the proton on the CO closest to the imidazole group, i.e., that of the Phe residue. This choice is justified by the fast proton transfer between the protonated imidazole and this carbonyl group at $\sim t = 0$. Figure S1 of the SI shows the two starting points and their evolution as a function of time, illustrating the fast proton transfer (~ 1 ps) from the imidazole to the CO sites. After activation of the reagent and a graph-based analysis of the ensemble of trajectories, the simultaneous fit of the population of the states, carried out using the three-state model, allows the rate constants depicted in Figure 6 to be extracted. All the rate constants obtained are summarized in Table S2 of the SI. The model reproduces the temporal evolution of the three states at their given total energy, as shown in Figure 6 (top). In all cases, the population of the reagent S monotonically decreases, while the product P population steadily increases. The population of the intermediate state I increases to a maximum, and then decreases. The RRK theory accurately reproduces the effective microcanonical rate constants as a function of the kinetic energy of the starting

state S, as shown in Figure 6 (bottom). Overall, the rate constants increase with the energy for the three systems, except for the backward reaction from the intermediate I to the reagent S. This may be due to the low activation energy required.

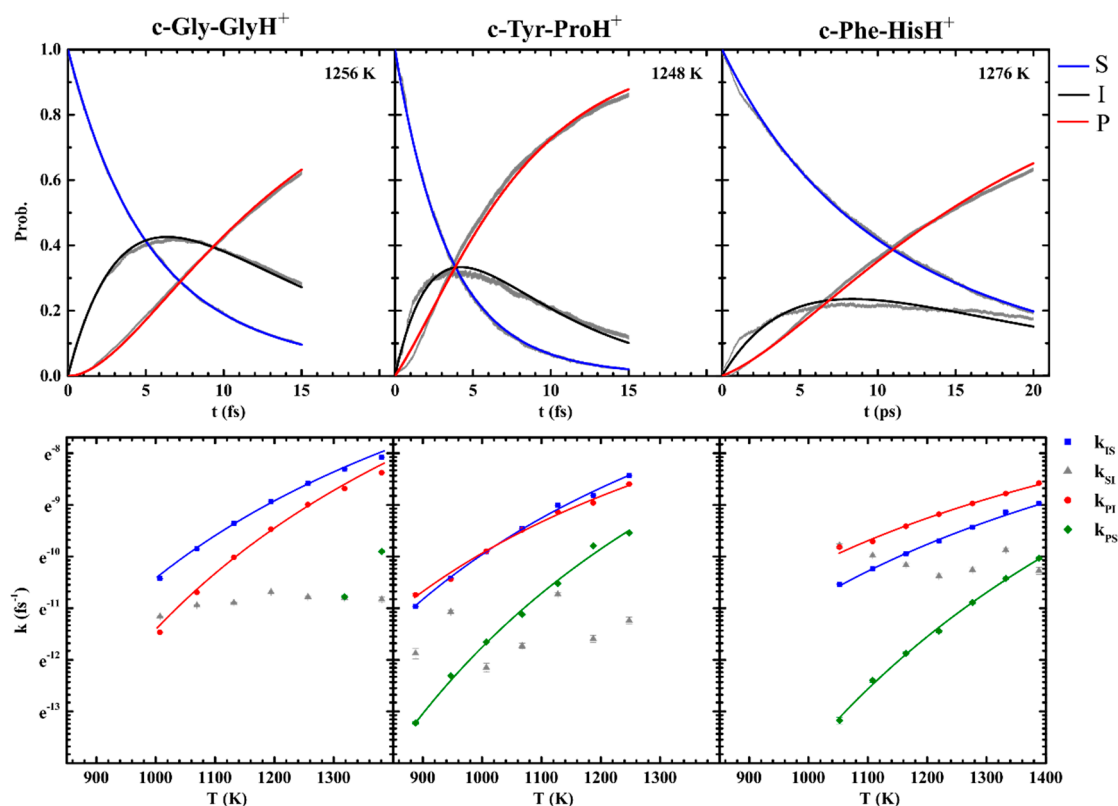


Figure 6. Top: Time evolution of the population of the different states (gray lines) fitted by the three-state model (colored lines: blue is the reagent S, grey the intermediate I, and red the product P). Bottom: Microcanonical rate constants (dots) extracted from chemical dynamics simulations using simultaneous fit approach and the classical RRK fit (solid lines) as a function of the kinetic temperature, defined as $E = n k_b T$, where n is the number of vibrational degrees of freedom. k_{IS} (blue squares) is the rate constant for the transformation from the starting point S (reagent) to the intermediate state I, while k_{SI} (grey triangles) is the rate constant for the reverse transformation. k_{PI} (red circles) is the rate constant for the transformation from the intermediate state I to the final state P (product). k_{PS} (green diamonds) is the rate constant for the direct transformation from the reagent to the product.

Analyzing the different rate constants allows us to obtain a global picture of the reactivity of the three systems investigated here, and to conclude that primary fragmentation occurs differently for the three systems. For c-Gly-GlyH⁺, $k_{IS} > k_{PI}$, which means that direct reactions are rare; the limiting step for stepwise reactions is the transformation of intermediate states I to products P. In contrast, for c-Phe-HisH⁺, $k_{PI} > k_{IS}$, indicating that the kinetically limiting step is the isomerization from the reactants S to the intermediate state I. Finally, $k_{IS} \sim k_{PI}$ for c-Tyr-ProH⁺ and their ratio depend on the excess energy. At low energy, the limiting step is the evolution from intermediate I to the products P. In contrast, at higher energy, it is the isomerization from the reactants S to the intermediate state I. In the energy range investigated here, events involving a direct reaction from the reagent S to the product P are scarce for c-Gly-GlyH⁺. In contrast, replacing Gly with Tyr, Phe, or His inherently opens the direct reaction channel, associated with the loss of the side chain, with no prior isomerization.

The obtained threshold energies for the different ionization steps are summarized in Figure 7, and are listed in Table S3 of the SI. We can first compare the energy thresholds for the various processes. The energy threshold for going directly from the reagent to the

product is always larger than that for going from the reagent to the intermediate state or the intermediate step to the product, demonstrating that the reaction is mostly stepwise. We can also compare the different systems. $c\text{-Gly-GlyH}^+$ and $c\text{-Tyr-ProH}^+$ have similar energy thresholds for isomerization when going from the reactants to the intermediate state. This could be related to the fact that the main isomerization events in both systems consist of the opening of the DKP ring, due to the breaking of the $C_\alpha\text{-COH}^+$ bond [10,35]. The energy threshold between the intermediate and final states is 12 kcal/mole lower in $c\text{-Tyr-ProH}^+$ than $c\text{-Gly-GlyH}^+$.

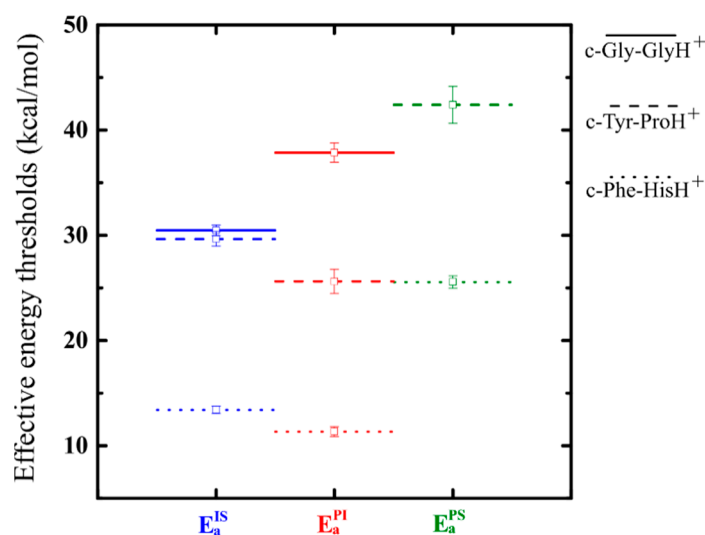


Figure 7. Comparison between the extracted effective energy thresholds (in kcal/mol) for the three different systems. Protonated $c\text{-Gly-Gly}$, $c\text{-Tyr-Pro}$, and $c\text{-Phe-His}$ are shown in full lines, dashed lines, and dotted lines, respectively. The energy thresholds for going from the reagent to the intermediate (E_a^{IS}), from the intermediate to the product (E_a^{PI}), and directly from the reagent to the products (E_a^{PS}) are given in blue, red, and green, respectively.

This observation illustrates the influence of the nature of the residues in facilitating fragmentation from the intermediate state. $c\text{-Phe-HisH}^+$ has much lower energy thresholds, suggesting a different reaction mechanism, in line with what was previously suggested [10]. This difference is related to the different protonation site in $c\text{-Phe-HisH}^+$, which is not on the amide CO as in the other studied systems, but on the imidazole ring. Therefore, different intermediate states are calculated for $c\text{-Phe-HisH}^+$ and the two other systems, a selection of which are shown in Figure 8. In the paradigm system $c\text{-Gly-GlyH}^+$, open (linear) structures are the main intermediate states. The same is true for $c\text{-Tyr-ProH}^+$. In contrast, cyclic intermediate states exist in $c\text{-Phe-HisH}^+$. This has considerable effects on the dissociation pathways, in particular, their sensitivity to stereochemical factors. The protonated imidazole ring acts as a proton shuttle to different possible protonation sites, facilitating isomerization and fragmentation, as illustrated in Figure 8c. This explains the much lower energy threshold observed in $c\text{-Phe-HisH}^+$ and the sensitivity to stereochemical factors. This can be related to the much larger fragmentation efficiency observed for $c\text{-Phe-HisH}^+$, as shown in Figure 5.

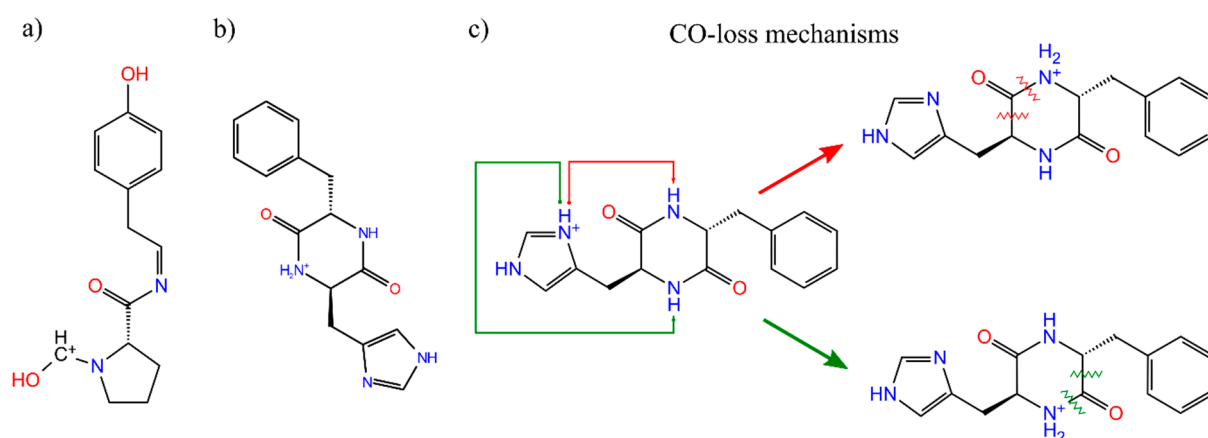


Figure 8. Intermediates and mechanism deduced from the simulations: (a) linear intermediate for protonated *c*-Tyr-Pro and (b) cyclic intermediate for protonated *c*-Phe-His. (c) Proton shuttling mechanisms explaining the sensitivity of CID to stereochemical factors in *c*-Phe-HisH⁺.

3.3. Effect of Symmetry and Chirality

For *c*-Tyr-ProH⁺, mainly linear intermediate states, similar to that shown in Figure 8a, are obtained. The evolution of the system from these intermediate states is the rate-limiting step at low collision energy, which corresponds to our experimental conditions. Therefore, the reaction rate k_{SP} is identical for the two diastereomers, because the open intermediate contains only one stereogenic center, which makes the reaction insensitive to chirality. For *c*-Phe-HisH⁺, the CO loss mechanism involves intermediate states that keep the DKP ring intact, with two asymmetric carbon atoms. The energy of the cyclic intermediate is, therefore, different whether the two chiral centers are of identical or opposite handedness, and so are the k_{IS} reaction rates. As mentioned before, k_{IS} is the rate-limiting step. One, therefore, expects different fragmentation efficiencies for LL and LD, in agreement with the experimental results shown in Figure 5. As illustrated in Figure 8c, the proton can shuttle through two possible pathways (shown here as red and green arrows), and the potential energy surface is not the same whether the residues are of identical or opposite handedness; this results in different CID efficiencies. This stereoselective mechanism dominates for CO loss and explains the stereoselectivity observed.

4. Conclusions

Here, we described the mechanisms of the collision-induced dissociation of protonated DKP dipeptides. The dominant neutral fragment is CO, the production of which involves the migration of the proton from the most stable protonation site to higher-energy protonation sites as a first step. The most symmetrical system, i.e., *c*-Gly-GlyH⁺, shows little direct reactivity from the initial to the final state. In this case, the limiting step is the transformation of intermediate states to products. Indeed, the most frequently encountered intermediate states are linear forms. The same holds for *c*-Tyr-ProH⁺, where disymmetrization of the system brings minor modifications, except an increase in the direct reaction rate. *c*-Phe-PheH⁺ has not been theoretically studied. However, the similarity between experimental results indicates strong similarity with *c*-Tyr-ProH⁺. In the two cases, the systems show two protonation sites that are similar in nature, which are the amide CO. They thus show similar CO loss reaction. This holds even when the system is not symmetrical, due to different conformations of identical substituents, such as in *c*-Phe-PheH⁺, or its chemical nature, such as in *c*-Tyr-ProH⁺. Reducing the symmetry of the system, by having different substituents, does not influence the reaction mechanisms. The change in the chirality of the residues does not influence the CID of these systems, and differences in the reactivity that are smaller than 10% are observed between LL and LD. Limited enantioselectivity is observed when the two residues differ in their chemical nature. In contrast, dramatic effects are present when the system is disymmetrized, due to the charge distribution, as in

c-Phe-HisH⁺. The proton location on the imidazole substituent enables a proton shuttling mechanism, in which the protonated imidazole rotates, in order to explore the different proton transfer possibilities. Due to stereochemical factors, the accessible conformational landscape is different for LL and LD. We conclude, from this work, that the dominant symmetry factor affecting the dependence of CID upon stereochemical factors is not the chemical dissymmetry induced by the nature of the residues, but the charge dissymmetry brought about by the proton location on a side chain.

Supplementary Materials: The following supporting information can be downloaded at: <https://www.mdpi.com/article/10.3390/sym14040679/s1>, Figure S1: (a) Starting point definition ($S = \text{str}^1 + \text{str}^2$) in c-Phe-HisH⁺ system due to the fast proton transfer detected during the chemical dynamics simulations. (b) Starting point population at 1276 K decomposed into its components. The inset highlights the fast proton transfer that takes place within 1 ps; Table S1: Details of the simulation. Λ is the total integration time, N the number of trajectories, E_v , the initial excess vibrational energy, $\langle K \rangle^{\text{SP}}$ the average kinetic energy of the starting point state and their corresponding standard deviations $\sigma_{\langle K \rangle}$. T^{SP} corresponds to the temperature computed from $\langle K \rangle^{\text{SP}}$. Table S2: Microcanonical rate constants and their corresponding uncertainty extracted from chemical dynamics simulations by a simultaneous fit approach using the three-state model. χ^2_{red} is the reduced chi-square per degree of freedom evaluating the quality of the fit. Table S3: Effective frequencies factors (in fs⁻¹) and energy thresholds (in kcal/mol) extracted from a fit using the RRK model.

Funding: This research was funded by the French National Agency (ANR) grant number ANR-14-CE06-0029-01.

Data Availability Statement: The data that support the findings of this study are available on request from the corresponding authors.

Acknowledgments: AFPM and RS thank the ANR DynBioReact contract (Grant No. ANR-14-CE06-0029-01) for financial support.

Conflicts of Interest: The authors declare no conflict of interest.

References

1. Bunker, P.R.; Jensen, R. *Molecular Symmetry and Spectroscopy*, 2nd ed.; NRC Research Press: Ottawa, ON, Canada, 1998.
2. Woodward, R.B.; Hoffmann, R. *The Conservation of Orbital Symmetry*; Academic Press: Cambridge, MA, USA, 1971.
3. Gal, J. Pasteur and the art of chirality. *Nat. Chem.* **2017**, *9*, 604–605. [[CrossRef](#)] [[PubMed](#)]
4. Milne, P.J.; Hunt, A.L.; Rostoll, K.; Van Der Walt, J.J.; Graz, C.J.M. The biological activity of selected cyclic dipeptides. *J. Pharm. Pharmacol.* **1998**, *50*, 1331–1337. [[CrossRef](#)] [[PubMed](#)]
5. Alata, I.; Perez-Mellor, A.; Ben Nasr, F.; Scuderi, D.; Steinmetz, V.; Gobert, F.; Jaidane, N.E.; Zehnacker-Rentien, A. Does the Residues chirality modify the conformation of a cyclo-dipeptide? Vibrational spectroscopy of protonated cyclo-diphenylalanine in the gas phase. *J. Phys. Chem. A* **2017**, *121*, 7130–7138. [[CrossRef](#)] [[PubMed](#)]
6. BenNasr, F.; Perez-Mellor, A.; Alata, I.; Lepere, V.; Jaidane, N.E.; Zehnacker, A. Stereochemistry-dependent hydrogen bonds stabilise stacked conformations in jet-cooled cyclic dipeptides: (LD) vs. (LL) cyclo tyrosine-tyrosine. *Faraday Discuss.* **2018**, *212*, 399–419. [[CrossRef](#)]
7. Perez-Mellor, A.; Alata, I.; Lepere, V.; Zehnacker, A. Chirality effects in the structures of jet-cooled bichromophoric dipeptides. *J. Mol. Spectrosc.* **2018**, *349*, 71–84. [[CrossRef](#)]
8. Pérez Mellor, A.; Zehnacker, A. Chirality effects in jet-cooled cyclic dipeptides. In *Physical Chemistry of Cold Gas-Phase Functional Molecules and Clusters*; Ebata, T., Fujii, M., Eds.; Springer: Singapore, 2019; pp. 63–87.
9. Perez-Mellor, A.; Alata, I.; Lepere, V.; Zehnacker, A. Conformational study of the jet-cooled diketopiperazine peptide cyclo tyrosyl-prolyl. *J. Phys. Chem. B* **2019**, *123*, 6023–6033. [[CrossRef](#)]
10. Perez-Mellor, A.; Le Barbu-Debus, K.; Lepere, V.; Alata, I.; Spezia, R.; Zehnacker, A. Structure and collision-induced dissociation of the protonated cyclo his-phe dipeptide: Mechanistic studies and stereochemical effects. *Eur. Phys. J. D* **2021**, *75*, 165. [[CrossRef](#)]
11. Perez-Mellor, A.; Le Barbu-Debus, K.; Zehnacker, A. Solid-state synthesis of cyclo LD-diphenylalanine: A chiral phase built from achiral subunits. *Chirality* **2020**, *32*, 693–703. [[CrossRef](#)]
12. Perez-Mellor, A.; Zehnacker, A. Vibrational circular dichroism of a 2,5-diketopiperazine (DKP) peptide: Evidence for dimer formation in cyclo LL or LD diphenylalanine in the solid state. *Chirality* **2017**, *29*, 89–96. [[CrossRef](#)]
13. Pérez Mellor, A.; Spezia, R. Determination of kinetic properties in unimolecular dissociation of complex systems from graph theory based analysis of an ensemble of reactive trajectories. *J. Chem. Phys.* **2021**, *155*, 124103. [[CrossRef](#)]
14. Nonappa; Ahonen, K.; Lahtinen, M.; Kolehmainen, E. Cyclic dipeptides: Catalyst/promoter-free, rapid and environmentally benign cyclization of free amino acids. *Green Chem.* **2011**, *13*, 1203–1209. [[CrossRef](#)]

15. Hirst, J.D.; Joakim Persson, D. Ab initio calculations of the vibrational and electronic spectra of diketopiperazine. *J. Phys. Chem. A* **1998**, *102*, 7519–7524. [[CrossRef](#)]
16. Bettens, F.L.; Bettens, R.P.A.; Brown, R.D.; Godfrey, P.D. The microwave spectrum, structure, and ring-puckering of the cyclic dipeptide diketopiperazine. *J. Am. Chem. Soc.* **2000**, *122*, 5856–5860. [[CrossRef](#)]
17. Wang, D.; Gulyuz, K.; Stedwell, C.N.; Polfer, N.C. Diagnostic NH and OH Vibrations for oxazolone and diketopiperazine structures: B(2) from protonated triglycine. *J. Am. Soc. Mass Spectrom.* **2011**, *22*, 1197–1203. [[CrossRef](#)] [[PubMed](#)]
18. Sletten, E. Conformation of cyclic dipeptides. The crystal and molecular structures of cyclo-D-alanyl-L-alanyl and cyclo-L-alanyl-L-alanyl (3,6-dimethylpiperazine-2,5-dione). *J. Am. Chem. Soc.* **1970**, *92*, 172–177. [[CrossRef](#)]
19. Strickland, E.H.; Wilchek, M.; Horwitz, J.; Billups, C. Low temperature circular dichroism of tyrosyl and tryptophanyl diketopiperazines. *J. Biol. Chem.* **1970**, *245*, 4168–4177. [[CrossRef](#)]
20. Yamazaki, T.; Nunami, K.I.; Goodman, M. Cyclic retro-inverso dipeptides with two aromatic side chains. II. Conformational analysis. *Biopolymers* **1991**, *31*, 1513–1528. [[CrossRef](#)]
21. Maitre, P.; Le Caer, S.; Simon, A.; Jones, W.; Lemaire, J.; Mestdag, H.; Heninger, M.; Mauclaire, G.; Boissel, P.; Prazeres, R.; et al. Ultrasensitive first coupling of FTICR and FEL. *Nucl. Instrum. Methods Sect. A* **2003**, *507*, 541–546.
22. Bakker, J.M.; Besson, T.; Lemaire, J.; Scuderi, D.; Maitre, P. Gas-phase structure of a pi-allyl-palladium complex: Efficient infrared spectroscopy in a 7 T fourier transform mass spectrometer. *J. Phys. Chem. A* **2007**, *111*, 13415–13424. [[CrossRef](#)]
23. Wysocki, V.H.; Tsaprailis, G.; Smith, L.L.; Breci, L.A. Special feature: Commentary—Mobile and localized protons: A framework for understanding peptide dissociation. *J. Mass Spectrom.* **2000**, *35*, 1399–1406. [[CrossRef](#)]
24. Frison, G.; van der Rest, G.; Turecek, F.; Besson, T.; Lemaire, J.; Maitre, P.; Chamot-Rooke, J. Structure of electron-capture dissociation fragments from charge-tagged peptides probed by tunable infrared multiple photon dissociation. *J. Am. Chem. Soc.* **2008**, *130*, 14916–14917. [[CrossRef](#)] [[PubMed](#)]
25. Song, K.; Spezia, R. *Theoretical Mass Spectrometry: Tracing Ions with Classical Trajectories*; De Gruyter: Boston, MA, USA, 2018.
26. Meroueh, S.O.; Wang, Y.F.; Hase, W.L. Direct dynamics Simulations of collision- and surface-induced dissociation of N-protonated glycine. Shattering fragmentation. *J. Phys. Chem. A* **2002**, *106*, 9983–9992. [[CrossRef](#)]
27. Bleiholder, C.; Osburn, S.; Williams, T.D.; Suhai, S.; Van Stipdonk, M.; Harrison, A.G.; Paizs, B. Sequence-scrambling fragmentation pathways of protonated peptides. *J. Am. Chem. Soc.* **2008**, *130*, 17774–17789. [[CrossRef](#)] [[PubMed](#)]
28. Brodbelt, J.S. Ion activation methods for peptides and proteins. *Anal. Chem.* **2016**, *88*, 30–51. [[CrossRef](#)]
29. Bythell, B.J.; Suhai, S.; Somogyi, A.; Paizs, B. Proton-driven amide bond-cleavage pathways of gas-phase peptide ions lacking mobile protons. *J. Am. Chem. Soc.* **2009**, *131*, 14057–14065. [[CrossRef](#)]
30. Harrison, A.G.; Young, A.B.; Bleiholder, C.; Suhai, S.; Paizs, B. Scrambling of sequence information in collision-induced dissociation of peptides. *J. Am. Chem. Soc.* **2006**, *128*, 10364–10365. [[CrossRef](#)]
31. Tsaprailis, G.; Nair, H.; Somogyi, A.; Wysocki, V.H.; Zhong, W.Q.; Futrell, J.H.; Summerfield, S.G.; Gaskell, S.J. Influence of secondary structure on the fragmentation of protonated peptides. *J. Am. Chem. Soc.* **1999**, *121*, 5142–5154. [[CrossRef](#)]
32. Wells, J.M.; McLuckey, S.A. Collision-induced dissociation (CID) of peptides and proteins. In *Biological Mass Spectrometry*; Burlingame, A.L., Ed.; Elsevier: Amsterdam, The Netherlands, 2005; Volume 402, pp. 148–185.
33. Carra, A.; Spezia, R. In silico tandem mass spectrometer: An analytical and fundamental tool. *Chem.-Methods* **2021**, *1*, 123–130. [[CrossRef](#)]
34. Martin-Somer, A.; Martens, J.; Grzetic, J.; Hase, W.L.; Oomens, J.; Spezia, R. Unimolecular fragmentation of deprotonated diproline pro(2)-H (-) studied by chemical dynamics simulations and IRMPD spectroscopy. *J. Phys. Chem. A* **2018**, *122*, 2612–2625. [[CrossRef](#)]
35. Perez-Mellor, A.; Alata, I.; Lepere, V.; Spezia, R.; Zehnacker-Rentien, A. Stereospecific collision-induced dissociation and vibrational spectroscopy of protonated cyclo (Tyr-Pro). *Int. J. Mass Spectrom.* **2021**, *465*, 116590. [[CrossRef](#)]
36. Becke, A.D. Density-functional thermochemistry. III. The role of exact exchange. *J. Chem. Phys.* **1993**, *98*, 5648–5652. [[CrossRef](#)]
37. Goerigk, L.; Grimme, S. A thorough benchmark of density functional methods for general main group thermochemistry, kinetics, and noncovalent interactions. *Phys. Chem. Chem. Phys.* **2011**, *13*, 6670–6688. [[CrossRef](#)] [[PubMed](#)]
38. Halls, M.D.; Velkovski, J.; Schlegel, H.B. Harmonic frequency scaling factors for hartree-fock, S-VWN, B-LYP, B3-LYP, B3-PW91 and MP2 with the sadlej pVTZ electric property basis set. *Theor. Chem. Acc.* **2001**, *105*, 413. [[CrossRef](#)]
39. Rocha, G.B.; Freire, R.O.; Simas, A.M.; Stewart, J.J.P. RM1: A reparameterization of AM1 for H, C, N, O, P, S, F, Cl, Br, and I. *J. Comput. Chem.* **2006**, *27*, 1101–1111. [[CrossRef](#)] [[PubMed](#)]
40. Grimme, S. Accurate description of van der Waals complexes by density functional theory including empirical corrections. *J. Comput. Chem.* **2004**, *25*, 1463–1473. [[CrossRef](#)]
41. Hase, W.L.; Buckowski, D.G. Monte-carlo sampling of a micro-canonical ensemble of classical harmonic-oscillators. *Chem. Phys. Lett.* **1980**, *74*, 284–287. [[CrossRef](#)]
42. Verlet, L. Computer experiments on classical fluids.i. thermodynamical properties of lennard-jones molecules. *Phys. Rev.* **1967**, *159*, 98–103. [[CrossRef](#)]
43. Forst, W. *Theory of Unimolecular Reactions*; Academic Press: New York, NY, USA, 1973.
44. Hase, W.L.; Duchovic, R.J.; Hu, X.; Komornicki, A.; Lim, K.F.; Lu, D.-H.; Peslherbe, G.H.; Swamy, K.N.; Vande Linde, S.R.; Zhu, L.; et al. VENUS96: A general chemical dynamics computer program. *QCPE Bull.* **1996**, *16*, 43.

45. Stewart, J.J.P.; Fiedler, L.J.; Zhang, P.; Zheng, J.; Rossi, I.; Hu, W.-P.; Lynch, G.C.; Liu, Y.-P.; Chuang, Y.Y.; Pu, J.; et al. *MOPAC 5.022mn*; Department of Chemistry and Supercomputing Institute, University of Minnesota: Minneapolis, MN, USA, 2015.
46. Oomens, J.; Young, S.; Molesworth, S.; van Stipdonk, M. Spectroscopic evidence for an oxazolone structure of the b(2) fragment ion from protonated tri-alanine. *J. Am. Soc. Mass Spectrom.* **2009**, *20*, 334–339. [[CrossRef](#)]
47. Perkins, B.R.; Chamot-Rooke, J.; Yoon, S.H.; Gucinski, A.C.; Somogyi, A.; Wysocki, V.H. Evidence of diketopiperazine and oxazolone structures for HA b(2)⁽⁺⁾ ion. *J. Am. Chem. Soc.* **2009**, *131*, 17528–17529. [[CrossRef](#)]
48. Shek, P.Y.I.; Lau, J.K.-C.; Zhao, J.; Grzetic, J.; Verkerk, U.H.; Oomens, J.; Hopkinson, A.C.; Siu, K.W.M. Fragmentations of protonated cyclic-glycylglycine and cyclic-alanylalanine. *Int. J. Mass Spectrom.* **2012**, *316*, 199–205. [[CrossRef](#)]